JGR Space Physics

RESEARCH ARTICLE
10.1029/2024JA032834

Quasi-Diurnal Lunar Tide O_1 in Ionospheric Total Electron Content at Solar Minimum

Klemens Hocke[1,2], **Wenyue Wang**[1,2], **Mokhamad Nur Cahyadi**[3], **and Guanyi Ma**[4]

[1]Institute of Applied Physics, University of Bern, Bern, Switzerland, [2]Oeschger Centre for Climate Change Research, University of Bern, Bern, Switzerland, [3]Department Geomatics Engineering, Institut Teknologi Sepuluh Nopember, Surabaya, Indonesia, [4]National Astronomical Observatories, Chinese Academy of Sciences, Beijing, China

Key Points:

- Geographical and seasonal distribution of O_1 tidal amplitude is derived from world maps of ionospheric total electron content
- O_1 component is maximal in northern hemispheric winter over west coast of South America with maxima northward and southward of magnetic equator
- Quasi-diurnal O_1 tide is as strong as the semidiurnal lunar M_2 tide in the ionosphere

Correspondence to:
K. Hocke,
klemens.hocke@unibe.ch

Citation:
Hocke, K., Wang, W., Cahyadi, M. N., & Ma, G. (2024). Quasi-diurnal lunar tide O_1 in ionospheric total electron content at solar minimum. *Journal of Geophysical Research: Space Physics*, *129*, e2024JA032834. https://doi.org/10.1029/2024JA032834

Received 2 MAY 2024
Accepted 1 JUL 2024

Author Contributions:
Conceptualization: Klemens Hocke, Wenyue Wang, Mokhamad Nur Cahyadi, Guanyi Ma
Formal analysis: Klemens Hocke
Investigation: Mokhamad Nur Cahyadi, Guanyi Ma
Methodology: Klemens Hocke, Wenyue Wang, Mokhamad Nur Cahyadi, Guanyi Ma
Software: Klemens Hocke, Wenyue Wang, Guanyi Ma
Validation: Wenyue Wang, Mokhamad Nur Cahyadi, Guanyi Ma
Writing – original draft: Klemens Hocke
Writing – review & editing: Wenyue Wang, Mokhamad Nur Cahyadi, Guanyi Ma

Abstract For the first time, characteristics of the geographical and seasonal distribution of the quasi-diurnal lunar O_1 tide were derived from a time series of ionospheric total electron content (TEC) maps provided by International Global Navigation Satellite System Service (IGS). The data analysis is focused on solar minimum in 2008 and 2009 where disturbing influences of geomagnetic and solar activity were minimal. We found that the magnitude of the O_1 tide is as strong as the "dominant" semidiurnal lunar M_2 tide. Relative amplitudes of 10% and larger are observed in some regions for the O_1 component in TEC. The O_1 component is particularly strong in northern hemispheric winter over the west coast of South America. There, two maxima occur which are northward and southward of the magnetic equator in the Equatorial Ionization Anomaly (EIA) crest regions. Following Yamazaki et al. (2017, https://doi.org/10.1002/2017ja024601), it might be assumed that a longitudinal anomaly of ionospheric conductivities in the Peruvian sector leads to a stronger modulation of the equatorial electrojet by the lunar tides. Electrodynamic lifting of plasma and transport to the EIA crests may explain the variations of the O_1 component in TEC. Contrary to many studies, we find the O_1 component (period 25.82 hr) more important than the M_1 component (period 24.84 hr, a lunar day). We show that the geographical distribution of the O_1 component is totally different from that of the M_1 component which is smaller. The seasonal variation of O_1 shows maximal amplitudes in northern hemispheric winter and minimal amplitudes in southern hemispheric winter.

1. Introduction

The quasi-diurnal lunar O_1 tide is observed in the ocean (e.g., sea level), in the atmosphere (e.g., surface pressure), in the ionosphere (e.g., electron density) and in the geomagnetic field at ground and in space. The O_1 tide is mainly due to the declination of the Moon. The period of the O_1 component is at about 25.82 hr according to a list of oceanic tidal constituents derived from tidal theory in Li (2022). The same period of the O_1 component was also found in a spectral analysis of a long-term time series of ground magnetometer data in Honolulu (Love & Rigler, 2014). In addition, the same period has been observed in ionospheric F_2 region electron density maximum *NmF*2 data at Okinawa (Hocke et al., 2024). The period of O_1 is different from a lunar day (24.84 hr) since the gravitational potential depends on both, the Moon and the Sun. In so far, the term luni-solar variation is often used for the lunar tidal variations (Malin & Chapman, 1970a).

The present study is focused on the O_1 tide which shows up in ionospheric total electron content. The plasma variation is due to the ionospheric dynamo due to the interactions of tidal neutral winds with the ionospheric layer. In addition, tidal breaking and dissipation in the lower thermosphere and thermal conduction induce temperature variations in the ionosphere and thermosphere which have an effect on the recombination rate of ions (Zolotukhina et al., 2011). Tidal breaking has a mixing effect on the neutral composition of the thermosphere, which affects the production and loss rates of ionospheric plasmas (Yamazaki & Richmond, 2013). The mixing effect is now considered to be an important mechanism for tidal influences on the ionosphere (Oberheide et al., 2020; Pedatella et al., 2016). The upward propagating O_1 tide in the atmosphere is supposed to have a large vertical equivalent depth of 26.5 km of the Hough eigenfunction (Tarpley, 1971). The vertical wavelength of the O_1 tide is about 300 km in the dynamo region, so that a considerable ionospheric plasma variation is generated (Tarpley, 1971).

Forbes and Zhang (2019) raised the question if the O_1 tide plays a role in the atmosphere. Indeed, we only found one observational article about a significant atmospheric O_1 tide in surface pressure in Hongkong (Malin & Chapman, 1970b). The lunar tidal potential of the O_1 tide is about 41.5% of those of the semidiurnal M_2 tide

(Tarpley, 1971). An indication of a strong ionospheric O_1 tide was given by Hocke et al. (2024) who found that the relative amplitude of O_1 in *NmF*2 is up to 12% for O_1 in winter above Okinawa. This was slightly higher than for the coincident observation of the semidiurnal lunar M_2 tide which is much better investigated than the O_1 tide in the ionosphere. Jones and Jones (1950) found a diurnal lunar tide in the high-latitude F_2 region by using ionosonde data. Pedatella (2014) also investigated a diurnal lunar tide in the ionosphere. They fitted a sine wave with the period of a lunar day to the observations (M_1 tide). We assume that the results for the M_1 tide are quite different than for the O_1 tide. Pedatella (2014) mentioned that significant contributions of non-migrating components of M_2 were contained in the ionospheric total electron content data.

Evidence for the atmospheric O_1 tide has been obtained in several studies about the geomagnetic O_1 tide. The analysis of geomagnetic lunar tides is complicated since they are generated by tidal electric currents in the ionosphere and in the ocean. The ocean dynamo is due to ions in the sea water which are moved by oceanic tides across the geomagnetic field lines. The generated electric currents contribute to the lunar geomagnetic tides which are observed by magnetometers. Malin (1970) described how the ionospheric and oceanic contributions to the geomagnetic lunar tides can be separated and that both sources generate important contributions to the ground magnetometer measurements. Significant contributions of the atmospheric O_1 tide (via the ionospheric dynamo) were derived from ground magnetometer data in several studies in the 1970s (Arora, 1979; Rao & Sastri, 1974; Winch, 1970).

It was observed and simulated that lunar tides are amplified in the upper atmosphere by the occurrence of sudden stratospheric warmings (SSWs) (Forbes & Zhang, 2012). Yamazaki et al. (2012) found that the geomagnetic lunar tide at the geomagnetic equator is enhanced in 70?% of the SSW events. The role of lunar and solar tidal variability in the generation of the ionospheric effects of SSWs is still under investigation. Hocke et al. (2024) observed an increase of the O_1 component in TEC during and after SSWs. The SSW-induced increase of the lunar amplitude is superposed on the general increase of the lunar tidal amplitude during Northern Hemisphere winter.

The present article will investigate the behavior of the O_1 tide in ionospheric total electron content. The spectral analysis which we perform does not distinguish between migrating and non-migrating O_1 tides. Our aim is to get a first impression on the global and seasonal distribution of the O_1 tide. We selected the year 2008 at solar minimum in order to have less contaminations from ionospheric effects of solar and geomagnetic activity. Section 2 describes the data set and the data analysis. Section 3 presents the results. The discussion is in Section 4, and conclusions are in Section 5.

2. Data Set and Data Analysis

The ionospheric total electron content is monitored by the worldwide network of Global Navigation Satellite System (GNSS) ground receivers which receive the radio signals of the GNSS satellites. The International GNSS Service (IGS) provides world maps of vertical total electron content (VTEC) with a time resolution of 2 hr and a spatial resolution of 5° in longitude and 2.5° in latitude since 1998. The calculation and the error assessment of these TEC maps were described by Hernández-Pajares et al. (2009). Even over data sparse regions such as the oceans, the relative error of TEC is less than 20% compared to coincident satellite altimeter observations. Pedatella (2014) showed that the TEC maps of IGS can be used for the analysis of lunar tides in ionospheric TEC. In 2008/2009 (used time interval of the present study) the GNSS constellation (used for the TEC maps) consisted of about 31 operational GPS satellites from USA and about 18 operational GLONASS satellites from Russia. The number of IGS ground stations was about 400 (Dow et al., 2009).

The data analysis of the present study is based on Fast Fourier Transform (FFT) spectral analysis. The FFT spectrum is calculated from the TEC time series at each grid point. We select a 10 weeks time interval. The relative fluctuations are computed with respect to the arithmetic mean of the 10 weeks interval of TEC values at a grid point:

$$\Delta TEC_{i,j}(t) = \frac{TEC_{i,j}(t)}{<TEC_{i,j}(t)>} \cdot 100 \quad (1)$$

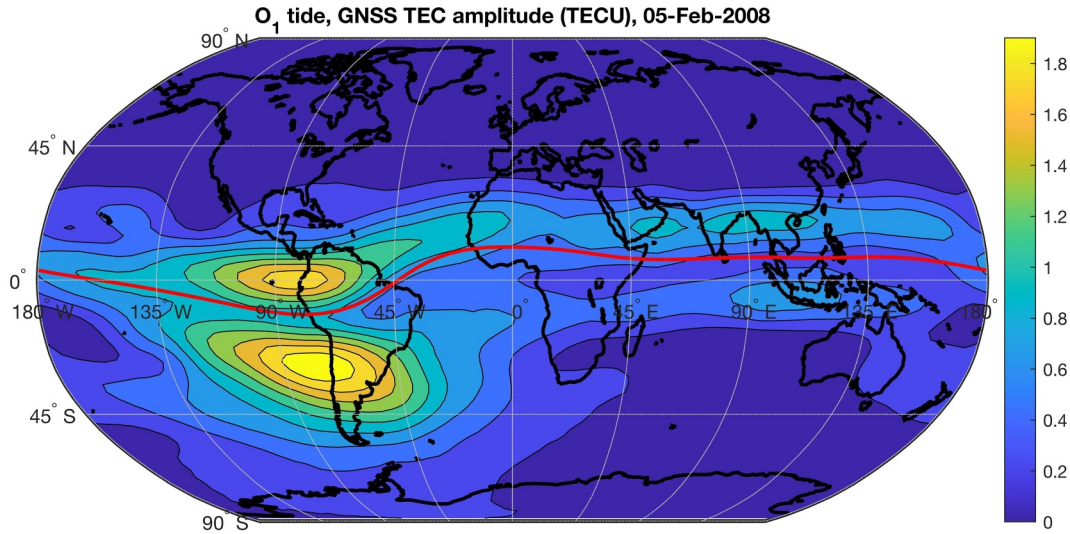

Figure 1. Absolute amplitude of the O_1 tide in TEC units. The time interval is at 2008-02-05 ± 5 weeks. The red line denotes the geomagnetic equator.

where $\Delta TEC_{i,j}(t)$ are the relative TEC fluctuations in percent, and i, j are the indices for the latitude and longitude of the grid point. $<TEC_{i,j}(t)>$ is the 10 weeks arithmetic mean over the time interval from $t_0 - 5$ weeks to $t_0 + 5$ weeks.

For absolute and relative TEC variations, we also subtract the arithmetic mean before the data segment is multiplied by a Hamming window. Then, we perform zero padding in order to achieve a high resolution of the FFT frequency grid. At each end of the data segment, we add 4 years with zeros, so that the frequency resolution of the FFT spectrum is 1.7×10^{-4} cycles per day (cpd). In addition, we tested with artificial sine waves (outgoing from similar 10 weeks interval of signal series as above) that the diurnal lunar tides O_1, M_1, M_2 and the solar tides S_1, S_2 can be well separated by our FFT analysis method. The involvement of the GNSS satellite system in the derivation of tidal constitutents can generate aliasing effects due to the revisit time of the GNSS constellation above a certain location on Earth. Biases of the K_1 and K_2 tidal constituents in sea level rise were found when the tidal measurements of tide gauges were compared to results of GNSS interferometric reflectometry (Peng et al., 2024). Note that the period of K_1 is equal to the GPS revisit period, which is 23.93 hr (one side-real day), and the period of K_2 is 11.97 hr, coinciding with the GPS orbital period. However, in the literature, there are no reports about possible biases for the O_1 tidal constituent which are resulting from the orbit parameters of the GNSS. Forbes and Zhang (2019) reported that the M_2 tide might be aliased by the O_1 tide but this is because they only used the CHAMP satellite for calculation of the M_2 tide in the upper atmosphere. In case of the present study, we use TEC data sampled by about 49 GNSS satellites. In so far, we are sure that the observed O_1 variation in GNSS TEC of the present study is not an aliasing effect. The O_1 variation was also observed by an ionosonde in Okinawa which does not depend on satellite orbits (Hocke et al., 2024).

Since zero padding and Hamming window reduce the amplitude of a signal in the FFT spectrum, we corrected the amplitude scale by means of an artificial sine wave of known amplitude. The selected FFT analysis of the TEC series is performed for each grid point separately. The disadvantage is that our analysis method does not separate between migrating and nonmigrating tidal components. The advantage is that our spectral analysis does not need assumptions about zonal wave numbers or propagation directions and speeds of the tides. The results of our analysis just show how strong the O_1 component in TEC is for an observer at a given location on ground.

3. Results

Figure 1 shows a world map of the absolute amplitude of the O_1 tide in TEC units (TECU). The 10 weeks time interval is centered at 2008-02-05. It is obvious that the O_1 tide is influenced by the geomagnetic field. The red line in Figure 1 depicts the geomagnetic equator, and one can see that the O_1 amplitude has maxima northward and southward of the geomagnetic equator. Further, the O_1 amplitude is maximal at the west coast of South

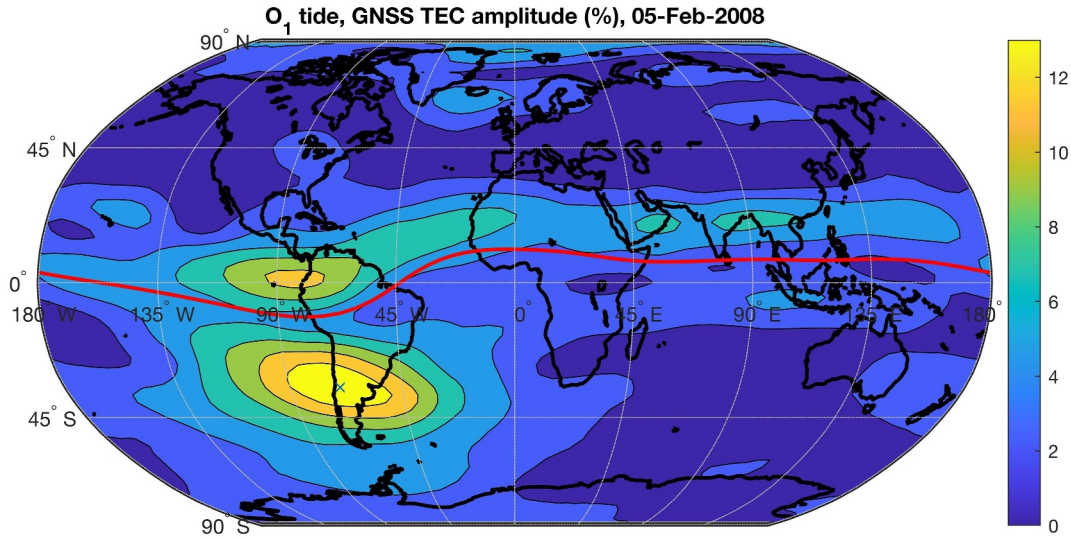

Figure 2. Relative amplitude of the O_1 tide in percent. The time interval is at 2008-02-05 ± 5 weeks. The red line denotes the geomagnetic equator.

America where the amplitude is up to 1.9 TECU. Please note that the IGS network of GNSS receivers has enough GNSS receivers at the west coast of South America, so that we can rely on the observed maxima of the lunar O_1 tide at the west coast of South America.

The geographical distribution of the relative amplitude of the O_1 tide is shown in Figure 2 and is quite similar to the world map of the absolute O_1 amplitude. In the following, we only focus on relative amplitudes where the relative amplitude is with respect to the 10 weeks mean of TEC at each grid point. The relative O_1 amplitude reaches maximal values of up to 13% at the west coast of South America. Figure 2 shows a green cross at the grid point 35°S and 70°W for which we show later a single FFT spectrum as example.

Before, we like to show that the world map of the M_1 (with period of a lunar day 24.84 hr) is quite different from that of the O_1 tide. Figure 3 shows the relative amplitude of the M_1 tide on 2008-02-05 which has maxima in the Arctic region with values up to 9%. The amplitude map of the semidiurnal M_2 tide (Figure 4) is quite similar to those of the O_1 tide (Figure 2). The spatial patterns and the magnitude of M_2 and O_1 are closely related.

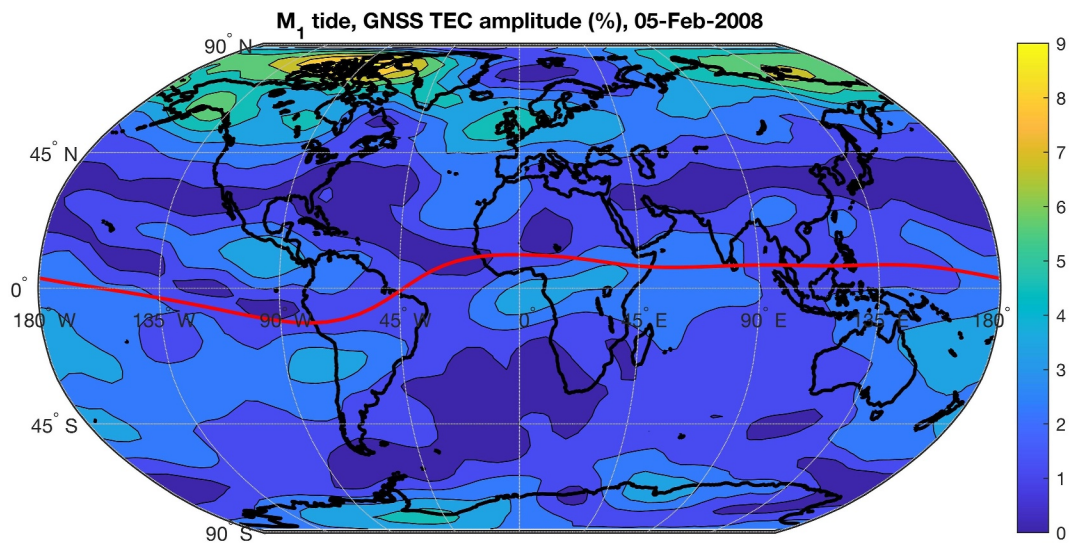

Figure 3. Relative amplitude of the M_1 tide in percent. The time interval is at 2008-02-05 ± 5 weeks. The red line denotes the geomagnetic equator.

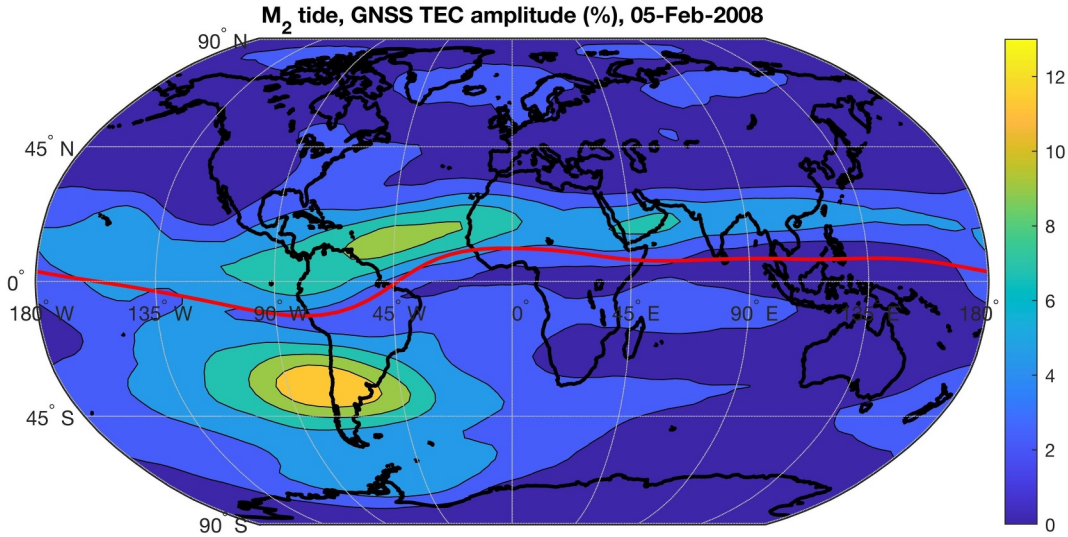

Figure 4. Relative amplitude of the M_2 (period: 12.42 hr) tide in percent. The time interval is at 2008-02-05 ± 5 weeks. The red line denotes the geomagnetic equator.

Figure 5 shows the FFT amplitude spectrum at the grid point 35°S and 70°W which was indicated by the green cross in Figure 2. The O_1 tide is a bit stronger than the M_2. The M_1 tide is not present at all. It is remarkable that the semidiurnal solar S_2 tide is smaller than the semidiurnal lunar M_2 tide.

The FFT spectrum also contains information about the phase of the O_1 tide. The phase is with respect to a fixed universal time. This is the start time of the FFT window which is equal for all grid points worldwide. Figure 6 shows the phase of the O_1 tide at 5 February 2008. The phase is calculated at each grid point. Generally, the phase of the O_1 tide depicts a zonal wavenumber 1 structure which is expected for a westward propagating quasi-diurnal tide.

Figure 7 shows the seasonal variation of the O_1 tide in 2008. It is obvious that the O_1 tide is strongest in February (Figure 7a) and weakest in August (Figure 7c). The O_1 tide in TEC is enhanced northward and southward of the geomagnetic equator which indicates a role of the plasma fountain effect for the amplification of O_1 in TEC.

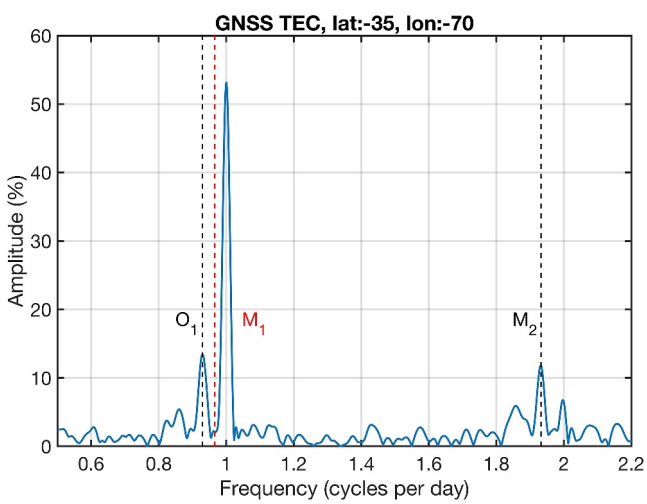

Figure 5. FFT amplitude spectrum at the grid point 35°S and 70°W on 2008-02-05 ± 5 weeks. The vertical dashed lines denote the frequency positions of the lunar O_1, M_1 (red) and the M_2 tide.

The clear pattern with the two maxima of O_1 at the west coast of South America is not only present in February 2008 but it is quite similar in February 2009 as Figure 8 shows. Similar to February 2008, a major SSW occurred on 24 January 2009 which certainly has an effect on the strength of O_1 in Figure 8. We show the result for February 2009 in addition to February 2008 in order to emphasize that the global distribution and the seasonal amplification of O_1 repeats from year to year.

Figure 9 compares the spectra of relative fluctuations of the F_2 peak electron density NmF2 of the ionosonde at Okinawa (blue line) with the coincident relative fluctuations of GNSS TEC (red line) for the time interval 2009-02-05 ± 5 weeks. It is obvious that the lunar tides O_1, M_2 and MK_3 occur in both data sets, so that we can exclude a satellite aliasing effect as explanation for their existence. The GNSS TEC spectrum has been magnified by a factor of 2, since the ionosonde NmF2 spectrum is larger than the GNSS TEC spectrum. We will see in the discussion that there are two possibilities to explain the origin of the O_1 and MK_3 component in NmF2 and GNSS TEC.

4. Discussion

First of all, the present study cannot decide about the origin of the O_1 component in ionospheric electron density. There are two possibilities. At

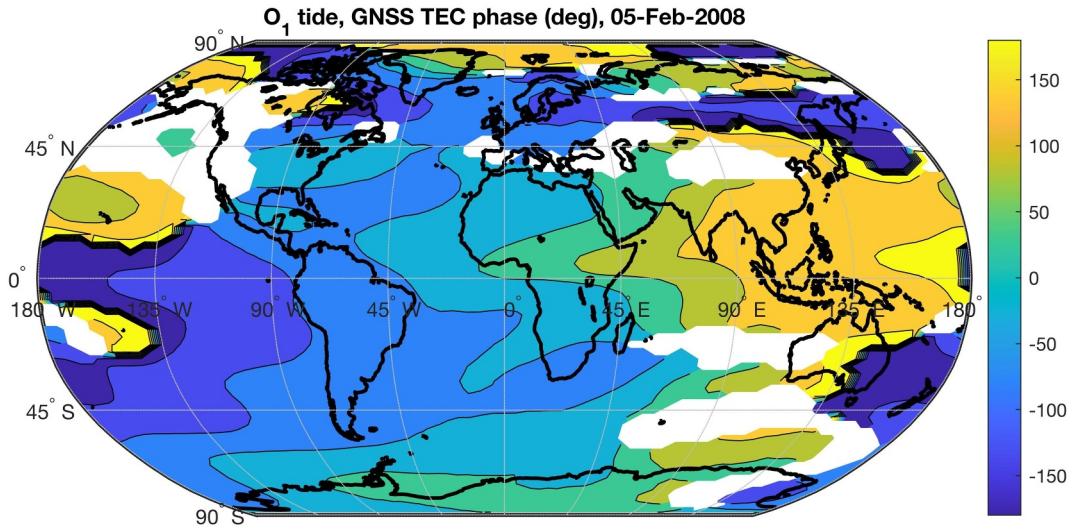

Figure 6. Global distribution of the phase of the lunar O_1 tide in TEC at 5 February 2008. The phase is derived from the FFT spectrum at each grid point independently. White color denotes regions where the relative amplitude of the O_1 tide is less than 1%.

first, a weak O_1 tide is excited by the Moon in the lower Earth's atmosphere. While the O_1 tide propagates upward its neutral wind fluctuations increases exponentially because of the decrase of the air density. In the lower thermosphere, O_1 wind amplitudes may reach 10 m/s or more and the O_1 tide may induce significant periodic variations in the plasma of the ionospheric F region. The drawback of this scenario is that there are no reports about a large O_1 neutral wind oscillation in the mesosphere and lower thermosphere.

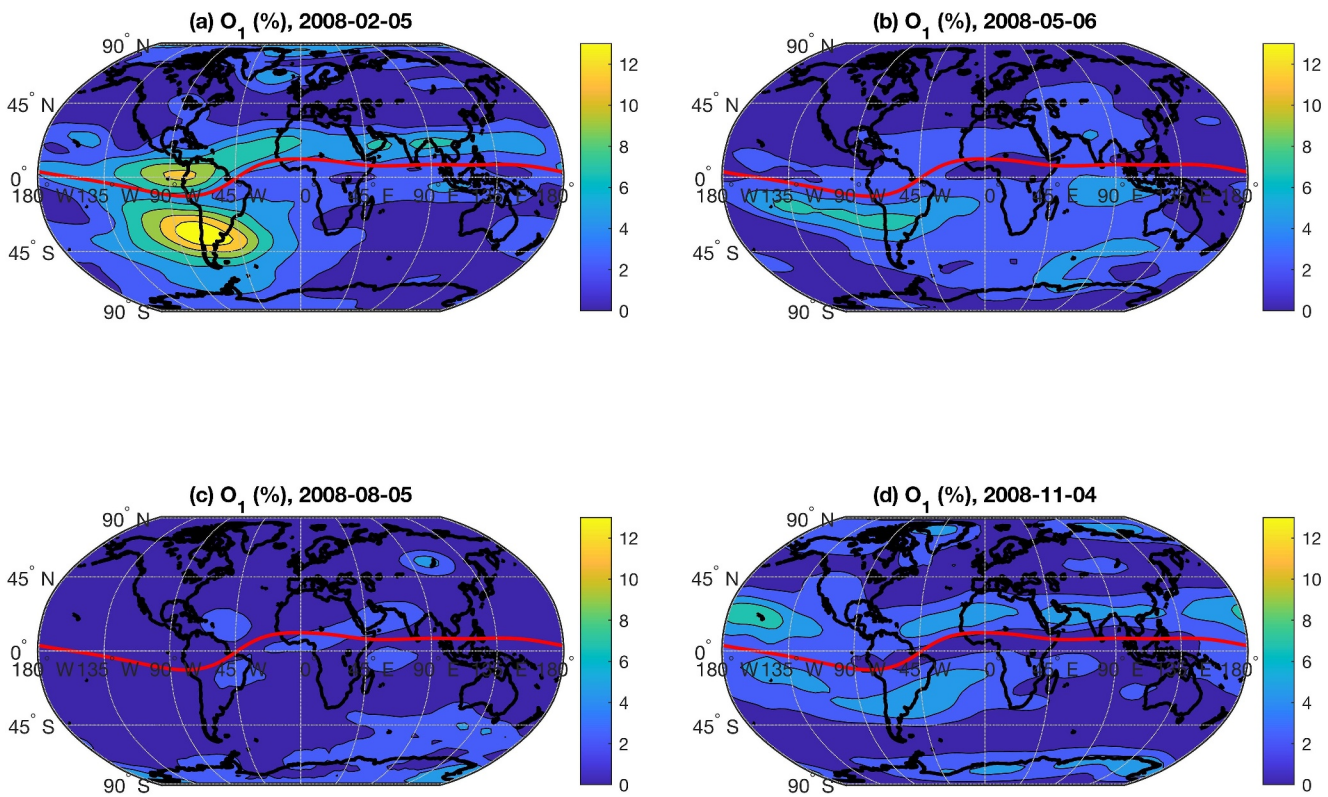

Figure 7. Seasonal variation of the relative amplitude of the O_1 tide. The time interval is at 2008-02-05 ± 5 weeks in (a), at 2008-05-06 ± 5 weeks in (b), at 2008-08-05 ± 5 weeks in (c), and at 2008-11-04 ± 5 weeks in (d). The red line denotes the geomagnetic equator.

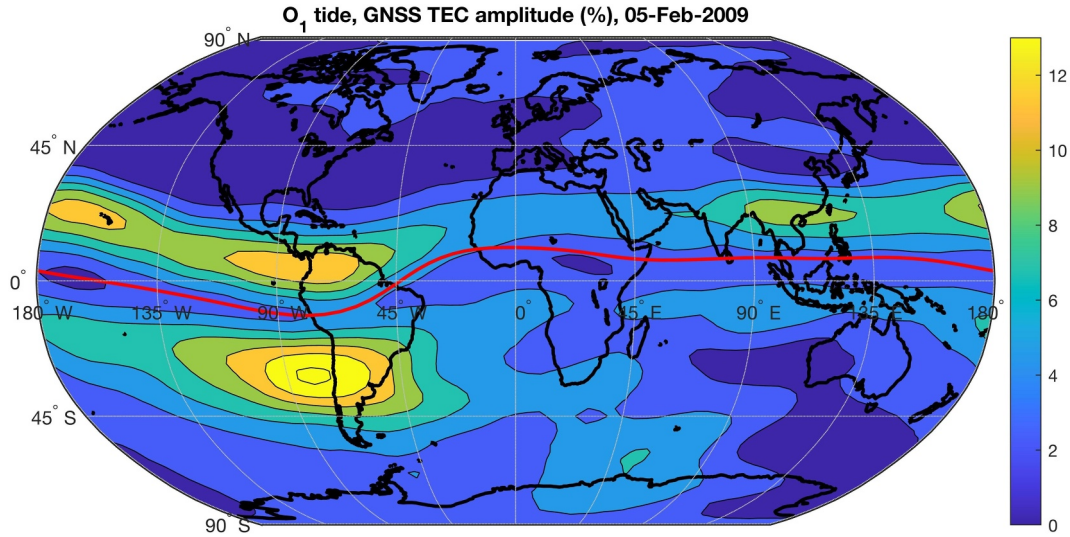

Figure 8. Relative amplitude of the O_1 tide in percent. The time interval is at 2009-02-05 ± 5 weeks. The red line denotes the geomagnetic equator. The global distribution of the O_1 amplitude is quite similar but a bit stronger than in the year before (Figure 2).

The second possibility was suggested by one of the reviewers. In the second case, the O_1 and MK_3 components are not excited in the lower atmosphere, but they are generated by a nonlinear interaction of the strong, lunar M_2 tide in neutral wind in the dynamo region (Zhang & Forbes, 2013) with the strong diurnal variation in ionospheric plasma density. The interaction of M_2 (12.42 hr period) and S_1 (24 hr period) generates oscillations at (1/12.42 + 1/24) cycles per day, or 8.18 hr period which is equal to the MK_3 period, and the other oscillation at (1/12.42−1/24) cycles per day, or 25.74 hr which is quite close to the O_1 period of 25.82 hr. The drawback of this scenario might be that O_1 and MK_3 would be expected quite smaller than the primary component M_2. However, in the present study O_1 and M_2 were of comparable size. For a further analysis of the origin of the observed O_1 component in the ionosphere, numerical simulations with a coupled atmosphere-ionosphere model would be necessary but this is beyond the scope of the present study. In addition, as already mentioned, a search for a possible O_1 tide in neutral wind observations of the lower thermosphere and below would be fine.

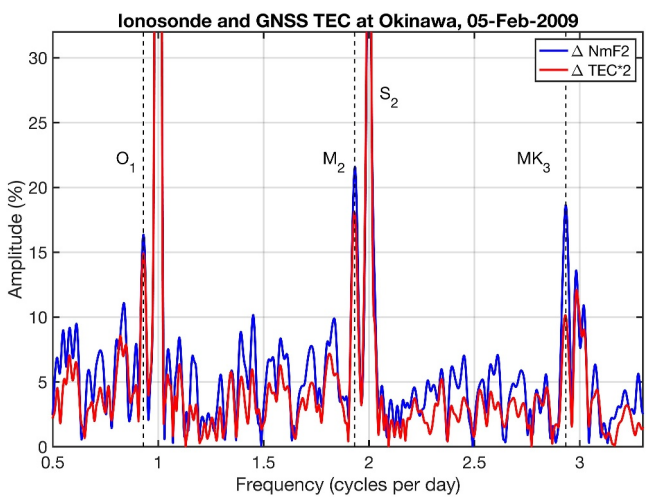

Figure 9. Spectrum of relative fluctuations of NmF2 (blue) and GNSS TEC (red) in percent. The location is Okinawa (26.7°N, 128.1°E), and the time interval is at 2009-02-05 ± 5 weeks. The spectrum of GNSS TEC has been magnified by a factor of 2. The vertical dashed lines indicate the frequencies of the lunar O_1, M_2, and MK_3 tidal constituents.

In the following discussion, we prefer the first case of interpretation, that an O_1 tide is generated in the lower atmosphere and amplified during its ascent to the upper atmosphere. Previous studies about the O_1 tide are mainly based on the geomagnetic lunar O_1 component (Arora, 1979; Rao & Sastri, 1974; Winch, 1970). However, these studies were usually at a few locations with ground magnetometers. In addition, the isolation of the atmospheric O_1 tide (ionosphere dynamo) from the oceanic O_1 tide (ocean dynamo) is difficult in case of the geomagnetic measurements. A FFT analysis of a time series of magnetic declination at Abinger in England did show a M_2 component but no spectral peak at the O_1 period (Black & Bullard, 1970). On the other hand, the geomagnetic data at Honolulu showed a strong O_1 spectral peak as well as M_2 (Love & Rigler, 2014). The latter two examples show that analysis of lunar tides in the frequency domain is a well recognized method.

The diurnal lunar M_1 tide in global maps of ionospheric TEC was studied by Pedatella (2014). However, we found that the global distribution of M_1 (Figure 3) is quite different from O_1 (Figure 2). In addition, the M_1 amplitude can completely vanish while the relative O_1 amplitude can exceed 10% (see spectrum in Figure 5). In the present study, we showed that the global distribution of the absolute O_1 amplitude (Figure 1) is quite similar to those of the relative amplitude (Figure 2). Thus, we focus on the discussion of the behavior of the relative O_1 amplitude in the following.

The present study was motivated by the findings of Hocke et al. (2024) who found strong lunar tides O_1 and M_2 in peak electron density data *NmF*2 above Okinawa with relative amplitudes of about 10%. It seems that the relative O_1 amplitude in the TEC map is smaller than 10% at the place of Okinawa (Figure 7). In agreement with the present study, Hocke et al. (2024) found that O_1 was enhanced from December to March. They showed that the maximal O_1 amplitudes occurred just after the onset of major SSWs. This is certainly a reason why it is important to learn more about the O_1 tide. The strong amplitudes of the O_1 tide indicate that knowledge of the O_1 tide is important for a description of the day-to-day variability of the ionosphere. For ionosphere and space weather models, it is important to include the gravitational effects of the moon and the sun on the Earth's atmosphere. In addition, the models have to simulate the vertical propagation of lunar tides from the ground to the ionosphere. The wind field in the middle atmosphere is assumed to have a strong effect on the propagation conditions of lunar and solar tides (Siddiqui et al., 2022).

The new result of the present study are the two maxima of the O_1 tide above the west coast of South America (Figures 2 and 8). The maxima are northward and southward of the geomagnetic equator. The reason for the locations of the maxima are unknown. A speculation might be that lower tropospheric air masses are shifted by lunar tidal winds against the Andean mountain ridge. This signal amplifies on the way up to the ionosphere, and the fountain effect (Hargreaves, 1992) leads to the formation of two ionization maxima northward and southward of the geomagnetic equator. This is similar to the well-known equatorial ionization anomaly (EIA) which has crests northward and southward of the geomagnetic equator. A decrease of the lunar tidal amplitude above the geomagnetic equator was also observed by Paulino et al. (2017) but for the semidiurnal tide M_2 in TEC maps above Brazil. We cannot compare the results for the diurnal lunar tide since Paulino et al. (2017) analyzed the M_1 component and not the O_1 component.

Another explanation for the maxima of the O_1 tide in northern hemispheric (NH) winter over the west coast of South America could be the longitudinal variation of ionospheric conductivities due to the inhomogeneous geomagnetic field. This explanation was provided by Yamazaki et al. (2017) who found that the lunar M_2 tide in the equatorial electrojet is enhanced in NH winter over the Peruvian sector. This observation is in agreement with our result about the longitudinal variation of the O_1 tide. The lunar modulation of the equatorial electrojet is strongest in the Peruvian sector, and periodic electrodynamic lifting of plasma above the magnetic equator leads to a lunar variation of TEC in the ionospheric EIA crest regions. Since there are GNSS receivers located along the Andean mountain range, the quality of the analyzed TEC data and the results of the O_1 tide over the west coast of South America are reliable. In addition, we obtain a quite similar amplitude distribution with similar maxima for the semidiurnal M_2 tide (Figure 4). This suggests that similar processes are involved in the generation of the O_1 and M_2 tide in TEC.

The phase distribution of the O_1 component in Figure 6 mainly indicates the dominance of a zonal wavenumber 1 tide. This is expected for a migrating diurnal tide such as the lunar O_1 tide. There are some deviations from the picture of a migrating lunar O_1 tide in the global distributions of amplitude and phase in Figures 2 and 6. The latitudinal and longitudinal anomalies of the amplitude and the phase may indicate the existence of non-migrating O_1 components. Another idea might be that geographical variations in the tidal propagation conditions may induce anomalies in the amplitude and phase maps observed in the ionosphere. The advantage of the present analysis which evaluates the TEC time series at each grid point independently is that the analysis method is sensitive to migrating, non-migrating and other waves. The only condition is that the oscillation has a period of 25.82 hr.

The seasonal variation of the O_1 tide is depicted in Figure 7. The color table has the same scale for all subfigures which correspond to the four different seasons. It is obvious that NH winter (Figure 7a) shows the strongest O_1 amplitude. Two maxima occur over the west coast of South America, northward and westward of the magnetic equator. We already discussed this behavior in detail. Compared to NH winter, the O_1 amplitude is much weaker in southern hemispheric (SH) winter (Figure 7c). This is in agreement with the observations of Yamazaki et al. (2017) obtained for the M_2 tide in the equatorial electrojet. In the most viewgraphs of Figure 7, we find indications that the patterns of the O_1 tidal amplitude follow the shape of the magnetic equator. This suggests that periodic electrodynamic lifting of plasma and accumulation of plasma above the EIA crests are most important for understanding of the lunar variations in TEC.

Finally, Figure 8 shows the result of the O_1 amplitude for 5 February 2009 which can be compared with the result for 5 February 2008 in Figure 2. The longitudinal and latitudinal variations which we already discussed before,

occur in both figures. The only significant difference is that the O_1 amplitude is stronger in February 2009 than in February 2008. This can be related to an amplification of the O_1 tide by the extraordinary major SSW of 24 January 2009. Forbes and Zhang (2012) analyzed the amplification of the M_2 and N_2 tides by the SSW of January 2009. They used CHAMP satellite data which cannot provide information about the O_1 tide. Hocke et al. (2024) showed in a composite analysis of 29 SSW events that the O_1 tide is amplified by major SSWs. The amplification of lunar tides by SSWs is a strong argument why space weather models should incorporate lunar tides, otherwise the day-to-day variability of the ionosphere and thermosphere system cannot be predicted adequately (Zhang et al., 2014).

5. Summary

For the first time, characteristics of the geographical and seasonal distribution of the quasi-diurnal lunar O_1 tide were derived from a time series of ionospheric TEC maps provided by IGS. The data analysis is focused on solar minimum in 2008 and 2009 where disturbing influences of geomagnetic and solar activity were minimal.

We found that the magnitude of the O_1 tide is as strong as the "dominant" semidiurnal lunar M_2 tide. Relative amplitudes of 10% and larger are observed in some regions for the O_1 component in TEC. The O_1 component is particularly strong in northern hemispheric winter over the west coast of South America. There, two maxima occur which are northward and southward of the magnetic equator in the EIA crest regions. Following Yamazaki et al. (2017), it might be assumed that a longitudinal anomaly of ionospheric conductivities in the Peruvian sector leads to a stronger modulation of the equatorial electrojet by the lunar tides. Electrodynamic lifting of plasma and subsequent transport to the EIA crests may explain the observed variations of the O_1 component in TEC.

Contrary to many studies, we find the O_1 component (period 25.82 hr) more important than the M_1 component (period 24.84 hr, a lunar day). We show that the geographical distribution of the O_1 component is totally different from that of the M_1 component which is in addition smaller. The seasonal variation of O_1 shows maximal amplitudes in northern hemispheric winter and minimal amplitudes in southern hemispheric winter.

The IGS TEC maps seem to be appropriate for exploring lunar tides in the ionosphere and for validation of lunar tides in whole atmosphere models. Lunar tides can contribute about 10% to the day-to-day variability of the ionosphere. The origin of the O_1 component in TEC remains an open question. It could be due to an upward propagating O_1 tide from the lower atmosphere, or it could be due to the nonlinear interaction between the M_2 tide and the diurnal variation in ionization.

Data Availability Statement

The TEC maps of the IGS are freely available at CDDIS, NASA's archive of space geodesy data https://cddis.nasa.gov/. The TEC maps are a product of the International GNSS Service (IGS) (Hernández-Pajares et al., 2009). The Okinawa ionosonde data are provided by the WDC for Ionosphere and Space Weather, Tokyo, National Institute of Information and Communications Technology at https://wdc.nict.go.jp/IONO/HP2009/ISDJ/manual_txt-E.html.

Acknowledgments
We thank the IGS and all contributors for maintaining the worldwide GNSS receiver network. We thank the WDC for Ionosphere and Space Weather, Tokyo, National Institute of Information and Communications Technology for providing the long-term *foF*2 series at Okinawa and for operation of the ionosonde. We thank one of the reviewers, Yosuke Yamazaki, for pointing out of a possible nonlinear interaction between the lunar M_2 tide and the diurnal variation in ionospheric plasma density. We thank both reviewers for their improvements and corrections. The Swiss National Science Foundation provided a shor-term research stay of Guanyi Ma at University of Bern (grant IZSEZO 224443). Open access funding provided by Universitat Bern.

References

Arora, B. R. (1979). O1 component of geomagnetic lunar daily variation at Alibag and its contamination by M2 component. *Journal of Geomagnetism and Geoelectricity*, *31*(2), 87–96. https://doi.org/10.5636/jgg.31.87

Black, D. I., & Bullard, E. C. (1970). Lunar and solar magnetic variations at Abinger: Their detection and estimation by spectral anaylsis via Fourier transforms. *Philosophical Transactions of the Royal Society of London - Series A: Mathematical and Physical Sciences*, *268*(1187), 233–263. https://doi.org/10.1098/rsta.1970.0074

Dow, J. M., Neilan, R. E., & Rizos, C. (2009). The international GNSS service in a changing landscape of global navigation satellite systems. *Journal of Geodesy*, *83*(3), 191–198. https://doi.org/10.1007/s00190-008-0300-3

Forbes, J. M., & Zhang, X. (2012). Lunar tide amplification during the January 2009 stratosphere warming event: Observations and theory. *Journal of Geophysical Research*, *117*(A12), A12312. https://doi.org/10.1029/2012JA017963

Forbes, J. M., & Zhang, X. (2019). Lunar tide in the F region ionosphere. *Journal of Geophysical Research: Space Physics*, *124*(9), 7654–7669. https://doi.org/10.1029/2019JA026603

Hargreaves, J. K. (1992). *The solar-terrestrial environment: An introduction to geospace - the science of the terrestrial upper atmosphere, ionosphere, and magnetosphere*. Cambridge University Press. https://doi.org/10.1017/CBO9780511628924

Hernández-Pajares, M., Juan, J. M., Sanz, J., Orus, R., Garcia-Rigo, A., Feltens, J., et al. (2009). The IGS VTEC maps: A reliable source of ionospheric information since 1998. *Journal of Geodesy*, *83*(3), 263–275. https://doi.org/10.1007/s00190-008-0266-1

Hocke, K., Wang, W., & Ma, G. (2024). Influences of sudden stratospheric warmings on the ionosphere above Okinawa. *Atmospheric Chemistry and Physics*, *24*(10), 5837–5846. https://doi.org/10.5194/acp-24-5837-2024

Jones, M. W., & Jones, J. G. (1950). Tidal effects in the ionospheric F-layer. *Journal of the Atmospheric Sciences*, *7*(1), 14–20. https://doi.org/10.1175/1520-0469(1950)007⟨0014:TEITIF⟩2.0.CO;2

Li, C. (2022). Harmonic analysis of tide. In *Time series data analysis in oceanography: Applications using matlab* (pp. 190–206). Cambridge University Press. https://doi.org/10.1017/9781108697101

Love, J. J., & Rigler, E. J. (2014). The magnetic tides of Honolulu. *Geophysical Journal International*, *197*(3), 1335–1353. https://doi.org/10.1093/gji/ggu090

Malin, S. R. C. (1970). 12). Separation of lunar daily geomagnetic variations into parts of ionospheric and oceanic origin. *Geophysical Journal International*, *21*(5), 447–455. https://doi.org/10.1111/j.1365-246X.1970.tb01781.x

Malin, S. R. C., & Chapman, S. (1970a). The determination of lunar daily geophysical variations by the chapman–miller method. *Geophysical Journal of the Royal Astronomical Society*, *19*(1), 15–35. https://doi.org/10.1111/j.1365-246X.1970.tb06738.x

Malin, S. R. C., & Chapman, S. (1970b). Lunar tidal components N_1 and O_2 in the atmospheric pressure. *Pure and Applied Geophysics*, *80*(1), 309–318. https://doi.org/10.1007/BF00880216

Oberheide, J., Pedatella, N. M., Gan, Q., Kumari, K., Burns, A. G., & Eastes, R. W. (2020). Thermospheric composition O/N response to an altered meridional mean circulation during sudden stratospheric warmings observed by GOLD. *Geophysical Research Letters*, *47*(1), e2019GL086313. https://doi.org/10.1029/2019GL086313

Paulino, A. R., Lima, L. M., Almeida, S. L., Batista, P. P., Batista, I. S., Paulino, I., et al. (2017). Lunar tides in total electron content over Brazil. *Journal of Geophysical Research: Space Physics*, *122*(7), 7519–7529. https://doi.org/10.1002/2017JA024052

Pedatella, N. M. (2014). Observations and simulations of the ionospheric lunar tide: Seasonal variability. *Journal of Geophysical Research: Space Physics*, *119*(7), 5800–5806. https://doi.org/10.1002/2014JA020189

Pedatella, N. M., Richmond, A. D., Maute, A., & Liu, H.-L. (2016). Impact of semidiurnal tidal variability during SSWS on the mean state of the ionosphere and thermosphere. *Journal of Geophysical Research: Space Physics*, *121*(8), 8077–8088. https://doi.org/10.1002/2016JA022910

Peng, D., Lin, Y. N., Lee, J.-C., Su, H.-H., & Hill, E. M. (2024). Multi-constellation GNSS interferometric reflectometry for tidal analysis: Mitigations for K1 and K2 biases due to GPS geometrical errors. *Journal of Geodesy*, *98*(1), 5. https://doi.org/10.1007/s00190-023-01812-3

Rao, D. R. K., & Sastri, N. S. (1974). The O1 component of the geomagnetic lunar daily variation in the Indian equatorial region. *Journal of Geomagnetism and Geoelectricity*, *26*(3), 285–293. https://doi.org/10.5636/jgg.26.285

Siddiqui, T. A., Chau, J. L., Stolle, C., & Yamazaki, Y. (2022). Migrating solar diurnal tidal variability during northern and southern hemisphere sudden stratospheric warmings. *Earth Planets and Space*, *74*(1), 101. https://doi.org/10.1186/s40623-022-01661-y

Tarpley, J. D. (1971). The O1 component of the geomagnetic lunar daily variation. *Journal of Geomagnetism and Geoelectricity*, *23*(2), 169–179. https://doi.org/10.5636/jgg.23.169

Winch, D. E. (1970). Geomagnetic lunar tides, o1 component. *Journal of Geomagnetism and Geoelectricity*, *22*(3), 319–328. https://doi.org/10.5636/jgg.22.319

Yamazaki, Y., & Richmond, A. D. (2013). A theory of ionospheric response to upward-propagating tides: Electrodynamic effects and tidal mixing effects. *Journal of Geophysical Research: Space Physics*, *118*(9), 5891–5905. https://doi.org/10.1002/jgra.50487

Yamazaki, Y., Richmond, A. D., & Yumoto, K. (2012). Stratospheric warmings and the geomagnetic lunar tide: 1958–2007. *Journal of Geophysical Research*, *117*(A4), A04301. https://doi.org/10.1029/2012JA017514

Yamazaki, Y., Stolle, C., Matzka, J., Siddiqui, T. A., Lühr, H., & Alken, P. (2017). Longitudinal variation of the lunar tide in the equatorial electrojet. *Journal of Geophysical Research: Space Physics*, *122*(12), 12445–12463. https://doi.org/10.1002/2017JA024601

Zhang, J. T., & Forbes, J. M. (2013). Lunar tidal winds between 80 and 110 km from UARS/HRDI wind measurements. *Journal of Geophysical Research: Space Physics*, *118*(8), 5296–5304. https://doi.org/10.1002/jgra.50420

Zhang, J. T., Forbes, J. M., Zhang, C. H., Doornbos, E., & Bruinsma, S. L. (2014). Lunar tide contribution to thermosphere weather. *Space Weather*, *12*(8), 538–551. https://doi.org/10.1002/2014SW001079

Zolotukhina, N. A., Pirog, O. M., & Polekh, N. M. (2011). Seasonal changes in the amplitude and phase of diurnal and semidiurnal variations in parameters of the midlatitude F2 layer under minimum solar activity conditions according to the data of an ionospheric station in Irkutsk (52.5°N, 104.0°E). *Geomagnetism and Aeronomy*, *51*(8), 1130–1137. https://doi.org/10.1134/S0016793211080330